Main Chain Conformation and Anomalous Elution Behavior of Cylindrical Brushes As Revealed by GPC/MALLS, Light Scattering, and SFM‡

Markus Gerle,† Karl Fischer, Sebastian Roos, Axel H. E. Müller, and Manfred Schmidt*

Institut für Physikalische Chemie, Johannes Gutenberg-Universität, Jakob-Welder-Weg 11, 55128 Mainz, Germany

Sergei S. Sheiko, Svetlana Prokhorova, and Martin Möller

Organische und Makromolekulare Chemie, Universität Ulm, 89069 Ulm, Germany

Received October 22, 1998; Revised Manuscript Received January 22, 1999

ABSTRACT: High molar mass polymacromonomers based on methacryloyl end-functionalized oligo methacrylates (M_n = 2410 g/mol) adopt the conformation of wormlike cylindrical brushes. Comparison of the absolute molar mass, M_w, determined by static light scattering and the contour length, L_w, of the molecules measured by SFM in the dry state revealed the length per vinylic main chain monomer of the cylindrical structure to be less than 0.1 nm, thus being much shorter than the maximum value of 0.25 nm. In solution this shrinkage could be quantified to 0.071 nm per monomer by Holtzer analysis of the scattering curves which in addition yielded the Kuhn statistical segment length l_k = 120 nm. GPC MALLS investigations of such samples showed an anomalous elution effect: After a regular elution at small elution volumes the molar mass of the eluting molecules increased drastically with increasing elution volume. Fractionation by GPC showed that this effect is caused by a fraction of extremely high molar mass molecules which elute by an unknown mechanism rather than by size exclusion.

Introduction

Polymacromonomers based on polystyrene[1,2] and poly(2-vinylpyridine)[3] side chains and a methacrylate main chain are known to adopt the conformation of cylindrical brushes caused by steric overcrowding of the side chains. Depending on the side chain length, the methacrylate main chain exhibits an extremely high chain stiffness on the order of 100 nm for the Kuhn statistical segment length. In the present paper we report on the preparation and characterization of polymacromonomers with chemically identical main and side chains based on methacrylates which were characterized by GPC/MALLS, by light scattering, and by SFM. Since the successful synthesis of "visible" macromolecules,[3−7] SFM has advanced to a powerful method not only to image macromolecules but also to determine molecular characteristics such as absolute molar masses, molar mass distribution, and chain conformation, i.e., chain stiffness, complementary to the advanced characterization in solution. In recent papers on poly(vinylpyridine) brushes[3] and on monodendron jacketed linear chains,[7] a significant discrepancy was reported between the light scattering molar masses and the molar masses derived from the contour length of the molecules determined by SFM assuming a fully stretched all-trans conformation of the vinylic main chain, i.e., 2.5 Å per monomer unit. To match the light scattering molar masses and the contour length of the cylindrical structure determined by SFM in the dry state, the average repeat length per monomer of the vinylic main chain l had to be significantly reduced to 1.2 Å ≤ l ≤ 2.3 Å depending on the "size" of the dendron as compared to the maximum and commonly adopted value of l = 2.5 Å. It was concluded[7] that the main chain is "locally coiled", but persistent on larger length scales in clear contradiction to Flory's "rotational isomeric state" model which predicts a "length scale independent" decay of the bond vector correlation function. Here we present an investigation on cylindrical brush molecules in solution with particular emphasis on the direct determination of the length per monomer via scattering techniques and compare these results to SFM measurements of the brush molecules in the dry state. We also address the question of whether SFM produces "ensemble average" properties in practice.

Experimental Section

PMMA macromonomers with a methacrylate end group were prepared by group transfer polymerization using a functionalized initiator as described elsewhere.[8] After purification of the macromonomers by flash chromatography the polymerization was conducted as described earlier:[2,9,10] 5 g of PMMA macromonomer and 2.5 mg of azobis(isobutyronitrile) (AIBN) were dissolved in 2.5 mL of benzene and polymerized at 60 °C for 3 days. The polymacromonomer was purified by precipitation in methanol (which still dissolves the unreacted macromonomer), redissolved in benzene, and freeze-dried. The number-average molar mass of the macromonomer was determined by MALDI-TOF to M_n = 2410 g mol^{-1} as described elsewhere[2].

The characterization of the polymacromonomers was performed by size exclusion chromatography equipped with a refractive index detector (Waters 410) and an ALV 1800 multiangle light scattering detector (MALLS) operating with an Ar ion laser (514 nm wavelength and 300 mW power) as described elsewhere.[2,11] The homemade, cylindrical flow cell exhibits a total volume of 38 μL. Size exclusion chromatogra-

† Present address: KPMG Unternehmensberatung GmbH, Olof-Palme-Str. 31, D-60439 Frankfurt/Main.

* To whom correspondence should be addressed.

‡ Dedicated to Prof. W. H. Stockmayer on the occasion of his 85th birthday.

10.1021/ma9816463 CCC: $18.00
Published on Web 03/27/1999

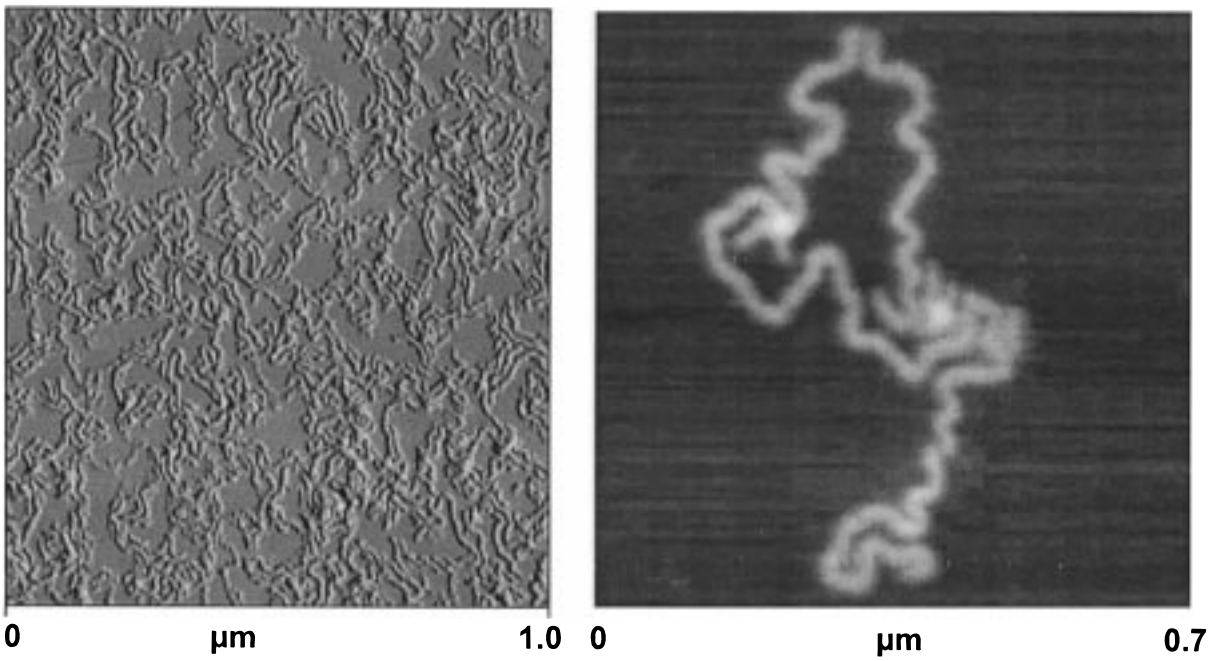

Figure 1. AFM picture of the unfractionated PMMA brushes: left side, amplitude; right side, magnification of single molecules in the height mode.

phy was performed in THF utilizing polystyrene gel columns (5 μm, 10^3 Å, 10^5 Å, 10^6 Å nominal pore diameter, PSS Co., Mainz) and a flow rate of 1 mL/min. Typically 100 μL of polymacromonomer (concentration 2−3 g/L) was injected. The shape of the chromatogram did not change for different injected concentrations. Thus, "overloading" of the columns can be excluded.

The fractionation of the PMMA polymacromonomer was achieved by accumulating 75 analytical GPC runs under conditions described above. From each GPC run four fractions were collected with a Gilson FC 205 fraction collector. The THF was evaporated, and the samples were dissolved in benzene and freeze-dried.

The samples for tapping mode SFM measurements were prepared by spin casting (2000 rpm) a dilute solution ($c = 0.15$ g/L) of the polymacromonomers in chloroform.

Scanning force micrographs were recorded at ambient conditions with a Nanoscope III instrument (Digital Instruments, St. Barbara, CA) operating in the tapping mode.[12] In this mode a cantilever with a sharp tip is oscillated by a piezo driver near its resonance frequency of about 300 kHz. As the tip taps the surface both the amplitude and the phase of the oscillation change, which allows recording of images with a topographic or viscoelastic contrast.[13−15] The Si probes had a spring constant of about 40 N m^{-1}.

Results and Discussion

In Figure 1 the SFM picture of the methacrylate polymacromonomers reveals a structural similarity to the polystyrene and poly(vinylpyridine) cylindrical brushes. The wormlike nature of the polymer is clearly visualized, and the curvature in terms of the Kuhn statistical segment length of the molecules could principally be analyzed. However, such a procedure does not appear meaningful in order to characterize the intrinsic stiffness as discussed for molecules in solution because (i) the molecules are confined to two dimensions and (ii) the molecular conformation is expected to be susceptible to the interaction with the surface. Moreover, the observed conformation might not even represent an equilibrium state because capillary forces may become dominant during solvent evaporation upon spin casting.

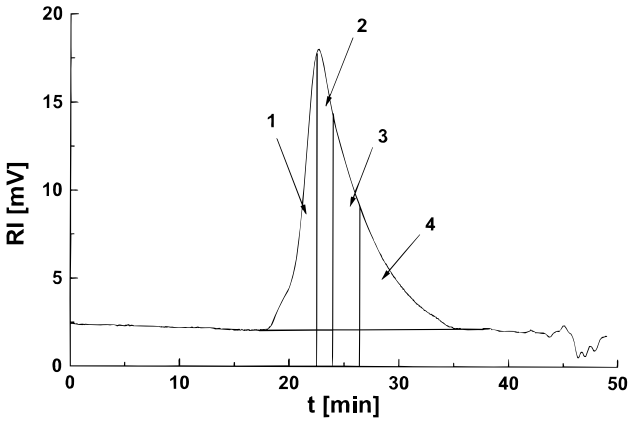

Figure 2. GPC trace of the PMMA brushes. The numbers indicate the collected fractions.

The GPC Anomaly. Following our earlier work on polystyrene polymacromonomers,[2] we utilized our GPC setup with refractive index (RI) and multiangle light scattering (MALLS) detection. In Figure 2 the concentration signal of the eluting molecules reflects the expected broad molar mass distribution along with a tailing toward large elution volumes, which usually would be interpreted as some low molar mass fraction. However, the light scattering signal reveals that at large elution volumes the apparent molar mass of the eluting molecules increases with increasing elution volume in contradiction to the normal size exclusion separation mechanism (see Figure 3). In the following the term "apparent" appreciates the fact that the usual extrapolation of the reduced scattering intensity vs q^2 might not yield the true molar mass and the true radius of gyration, respectively, because particularly for the large polymers $qR_g \gg 1$, which makes zero q extrapolations highly unreliable. This effect is quantitatively addressed in the Appendix and does not alter the qualitative conclusions drawn below from the apparent quantities. Only at small elution volumes is the normal size exclusion behavior observed qualitatively, i.e., decreas-

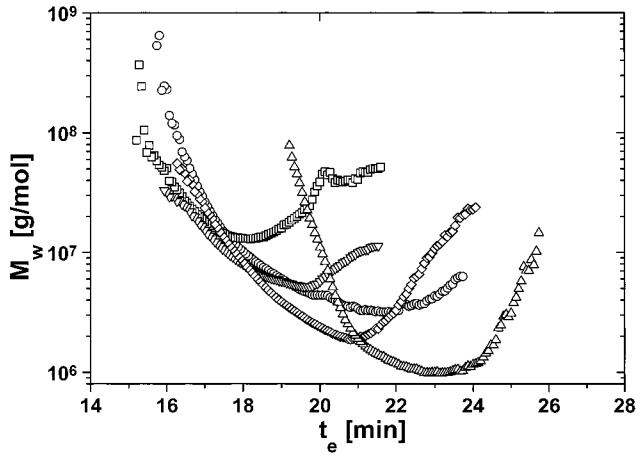

Figure 3. Apparent molar mass, M_w^{app}, as a function of the elution volume V_e for the unfractionated sample (○) and the fractions 1 (□), 2 (▽), 3 (◇), and 4 (△).

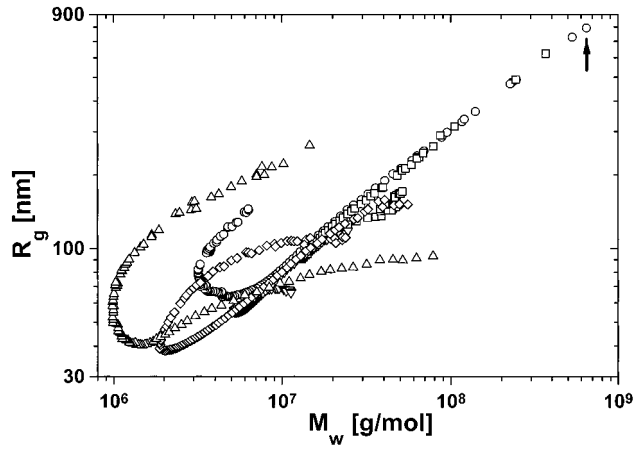

Figure 4. Apparent radius of gyration, R_g^{app}, vs the apparent molar mass, M_w^{app}. Symbols like in Figure 3.

ing apparent molar mass with increasing elution volume. It follows from Figure 3 that fractions of the sample with identical apparent weight-average molar masses elute at two different elution volumes. In Figure 4 the simultaneously determined apparent *z*-average mean-square radius of gyration $R_g^{app} \equiv \langle S^2 \rangle_z^{1/2}$(app) is plotted versus the molar mass M_w^{app} of the eluting molecules. The shape of the curve is extremely anomalous because R_g differs for identical M_w. The arrow in Figure 4 marks the beginning of the chromatogram of the unfractionated parent sample (○) at small elution volumes.

Phenomenologically, the anomaly is explained by the concomitant occurrence of two opposing separation mechanisms: the normal size exclusion where the molecules elute according to their hydrodynamic volume, i.e., large molecules elute first followed by the smaller ones, and an unknown, second separation mechanism where the large molecules are retarded, i.e., elute at large volumes where according to size exclusion only very small molecules are expected. Consequently, a small fraction of extremely large species coelute with the normally eluting small molecules, thus causing a bimodal molar mass distribution in each fraction of the eluting polymers. Particularly at high elution volumes the polydispersity of the eluting fractions could become extremely large. Since light scattering measures the *z*-average radius of gyration and the weight-average

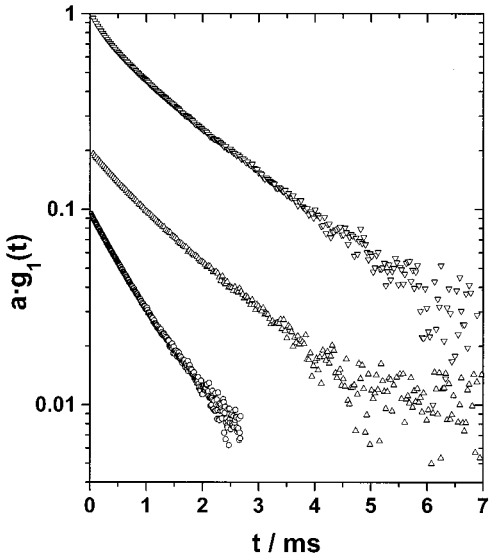

Figure 5. Typical correlation functions $g_1(t)$ recorded at 50° scattering angle which are shifted by an arbitrary factor *a*: fraction 1 (△, $a = 0.2$), fraction 2 (○, $a = 0.1$), and fraction 4 (▽, $a = 1$).

molar mass, the $R_g - M_w$ curve is shifted upward with increasing polydispersity which qualitatively explains the shape of the curve observed for the unfractionated sample in Figure 4. To prove the above hypothesis, the sample was fractionated as described above. The fractionation cutoffs are marked by arrows in Figure 2.

The explanation for GPC anomaly as discussed above is qualitatively confirmed by the static and dynamic light scattering results shown in Figure 5. Fractions 2 and 3 exhibit correlation functions which display a monomodal decay with moderate polydispersity (normalized second cumulant $0.08 \leq \mu_2 \leq 0.1$), yielding hydrodynamic radii of $R_h = 50$ nm and $R_h = 38$ nm, respectively. In contrast, the correlation functions of fraction 4 show a bimodal decay. The slower decay constant corresponds to a hydrodynamic radius of $R_h \approx 120$ nm, and the fast decay yields $R_h \cong 19$ nm. For the correlation functions of fraction 1 a bimodal decay cannot be convincingly postulated. Whereas the apparent diffusion coefficients $D_{app} \equiv \Gamma/q^2$ depend only slightly on the scattering angle for fractions 2 and 3, a strong dependence was observed for fraction 1 (a factor of 2 from 0° to 130° scattering angle). This may indicate a larger polydispersity of the sample which is also indicated by somewhat larger values of $\mu_2 = 0.10-0.12$ but could also originate from internal modes of motion which become more pronounced for larger chain length. It is also conceivable that extremely large molecules may be filtered out or break during filtration. A more detailed investigation of such subtle effects was prohibited by the extremely small amount of sample available ($\approx$1 mg).

Likewise, the static light scattering results exhibited unusually high uncertainties due to the weighing error. Eventually the concentration was determined via GPC by comparing the peak area of the refractive index signal of the light scattering samples to the peak area of linear PMMA of known concentration. Due to the small signals obtained, the concentration determination is accurate to $\pm$20%, only. At the small concentrations investigated ($c > 0.1$ g/L) this does not seriously affect the apparent radius of gyration, but rather the apparent molar mass. As will be discussed below in detail, also

Table 1. Light Scattering and SFM Characterization of the Polymacromonomer Fractions[a]

	$M_w^{app} \times 10^6$/g mol^{-1}	R_g^{app}/nm	R_h/nm	L_w^{SFM}/nm	L_n^{SFM}/nm	l_{SFM}^c/nm
F1	≈60[c]	170	103	640	485	0.026
F2	14	84	50	443	322	0.076
F3	7.5	70	38	254	193	0.081
F4 (comp 1)	1.7[c]		19	72	49	0.1
F4 (comp 2)	100[c]		120			

[a] Fraction 4 contains a low (comp 1) and a high molar mass component (comp 2). [b] Estimated from the hydrodynamic radius. [c] Length per monomer according to $l_{SFM} = L_w^{SFM} M_o / M_w^{app}$.

the extrapolation to zero q is highly ambiguous because of the large $u = qR_g$ values reached by the present samples. Even at 15° scattering angle u becomes larger than 1 for fractions 1 and 4, which makes a reliable extrapolation for the determination of M_w and R_g impossible. Therefore, we give a crude estimate of the molar masses of fractions 1 and 4 based on the hydrodynamic radii, because these are insensitive to incorrect concentrations and do not suffer strongly from zero q extrapolation problems. The static and dynamic light scattering results are summarized in Table 1.From the above results the GPC anomaly is qualitatively explained. It is, however, extremely difficult to trace the origin of the anomalously eluting large molecules. The obvious explanations comprise overloading of the columns, adsorption, and sieving. Overloading of the columns can be safely excluded, because the shape of the elution peak did not change upon reduction of the injected amount of sample by more than a factor of 10. Retardation by adsorption of the molecules onto the column material seems to be unlikely, because THF represents a very good solvent for PMMA. Also, linear PMMA coils elute completely regular. For large polymers with a radius of gyration of 100 nm and above the end-to-end distance reaches the order of 300−500 nm. This is close to the dimension of the voids between close-packed spheres of 5 μm diameter, particularly if the column material is squeezed by the high pressure. Accordingly, the largest molecules are forced to "reptate" through the voids between the polystyrene beads representing the column material. Such a mechanism, however, should provide an effective separation which seems not to be compatible with the similar radii observed for fraction 1 and for the high molar mass component in fraction 4. It should be noted that the anomalous elution described above is not unique to the presently described PMMA polymacromonomers. Polymacromonomers based on polypropylene,[16] stiff polymers with dendritic coats,[17] and stiff polyisocyanate helices[18] show a similar behavior as well as subcritically branched polystyrene![11] From several experiments on stiff polymers with dendritic coats[17] the anomalous elution was observed to be much more pronounced for the high molar mass samples and to eventually disappear for the small molar mass samples. Since both adsorption and sieving should become more pronounced with increasing molar mass, this experimental result cannot distinguish between the two elution mechanisms. At least two of the systems discussed above, the branched polystyrene in toluene and the present PMMA brushes in THF, are extremely unlikely to adsorb onto the cross-linked polystyrene beads representing the column material. Thus, we conclude that the size in combination with the molecular architecture causes the anomalous elution which may originate from sieving as discussed above or from entanglement effects within the pore structure of the column material.

SFM Characterization of the Fractions. To compare the light scattering molar masses to the contour length of the cylindrical brush molecules, the four fractions were investigated by SFM as shown in Figure 6a−d.

On a small scale inspection of the SFM pictures does not reveal an obvious reason for the anomalous elution behavior of the fractions; i.e., no bimodal distribution of the contour length is observed for fraction 4 in contradiction to the dynamic light scattering results discussed above. In Table 1 the light scattering molar masses of the fractions are compared to the contour lengths extracted from the SFM pictures which yields the length per monomer l_{SFM} unit via the known mass $M_o = 2410$ g/mol of the macromonomer

$$l_{SFM} = L_w^{SFM} M_o / M_w^{app} \quad (1)$$

The results for l_{SFM} lie in the range 0.076 nm ≤ l_{SFM} ≤ 0.1 nm for fractions 2, 3, and 4. For fraction 1 SFM obviously misses some large molecules which is caused either by the statistical inaccuracy, i.e., the limited number of monitored molecules as compared to the broad length distribution, or by fractionation during spin casting. This effect becomes even more pronounced for fraction 4 where the high molar mass species of the bimodal chain length distribution established by dynamic light scattering is completely absent in the SFM picture shown in Figure 6d. Under the assumption that the missing molecules exhibit a similar or larger molar mass than those of fraction 1, the number fraction of large species in fraction 4 is estimated to be certainly less than 10^{-3}. Thus, it might be a problem for SFM to detect an extremely small number fraction of high molar mass species due to the limited number of molecules observed. Indeed, a careful inspection of large-scale micrographs of fraction 4 reveals that very few "monolayer islands" do exist (see Figure 6e) which are composed of extremely large molecules as shown in Figure 6f. Qualitatively, this observation impressingly confirms the proposed bimodal distribution of fraction 4.

This example demonstrates that monitoring "ensemble averages" by SFM may suffer significantly by the limitation in the statistical accuracy and possibly by fractionation during sample preparation, i.e., spin casting. For the monomodal fractions 2 and 3 comparison of the light scattering molar masses and the SFM contour length yields a length per monomer l_{SFM} = 0.07−0.1 nm, in qualitative agreement with the results obtained for poly(vinylpyridine) brushes[3] and for monodendron jacketed polymers.[7] A similar conclusion is drawn from the cross-sectional dimensions of the brushes observed by SFM which were determined to a brush height $h = 4.7 \pm 0.2$ nm and a width of $d = 11 \pm 1$ nm. Assuming the density of a dry brush molecule to be identical to the bulk density of PMMA, $\delta_{PMMA} = 1.19$

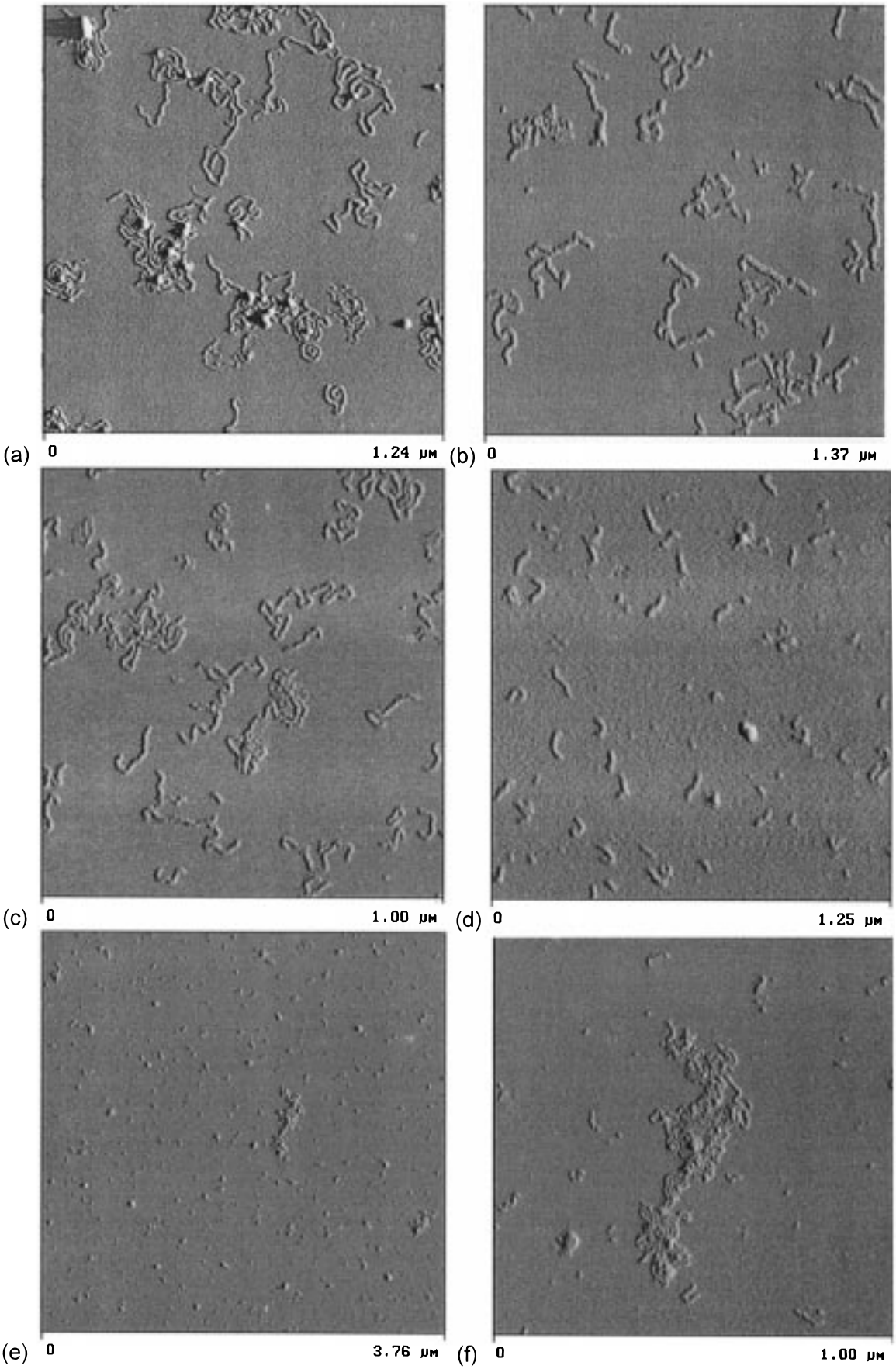

Figure 6. AFM pictures of the polymacromonomer fractions: fraction 1 (a), 2 (b), 3 (c), and 4 (d−f). The micrograph (e) represents a selected AFM picture of fraction 4 showing islands of large molecules, which is enlarged in (f).

g/cm^3, the length per monomer is calculated to $l_\delta = 0.084 \pm 0.01$ nm where an ellipsoidal cross section of the molecules is calculated according to $F = \pi hd/4$. Within experimental error l_{SFM} and l_δ both determined in the

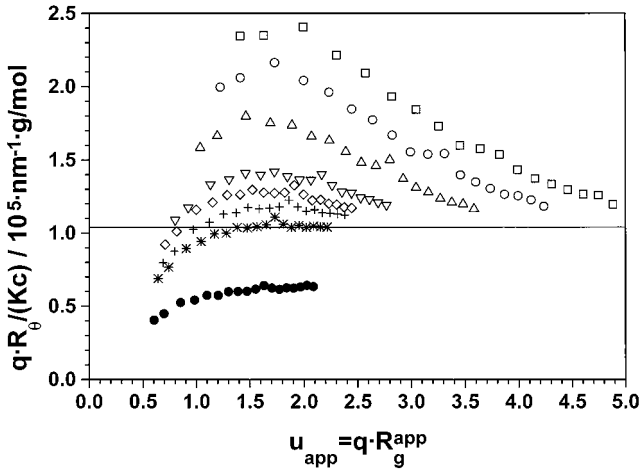

Figure 7. Holtzer plot of the light scattering data measured by GPC/MALLS of the unfractionated sample. The different curves correspond to molecules eluting at different volumes V_e: 16.8 mL (□), 17.0 mL (○), 17.3 mL (△), 18.0 mL (▽), 18.3 mL (◇), 18.7 mL (+), 19.0 mL (★), and 19.9 mL (●). For the discussion of the curve at $V_e = 19.9$ mL see Appendix.

dry state coincide and will now be compared to the absolute value of l of the dissolved molecules derived from static scattering results in the high q regime.

Determination of the Absolute Length per Monomer. The typical scattering behavior of semiflexible polymers at large values of the dimensionless quantity $u = qR_g$ principally allows the determination of M_L, the mass per unit length, and of l_k, the Kuhn statistical segment length. To reach high enough u values, only the extremely high molar mass molecules of the fractionated and of the unfractionated samples can be utilized for the precise analysis of the particle scattering factor. Therefore, additional GPC/MALLS measurements were performed on fractions 1−4, the results of which are included in Figures 3 and 4. All fractions elute more or less anomalously as expected from the discussion above. Particularly the elution behavior of fraction 4 is so strange that these data are excluded from the following discussion.

We now analyze the scattering envelopes of the GPC/MALLS data in terms of the well-known Holtzer plateau which principally allows the determination of M_L and l_k. This is shown in Figure 7 for the data of some GPC slices of the unfractioned sample, where qR_Θ/Kc is plotted versus the apparent quantity $u_{app} \equiv qR_g^{app}$. At small elution volumes, i.e., high molar masses, the data exhibit a pronounced maximum typical for semiflexible polymers whereas at large elution volume, i.e., small molar masses, a monotonically increasing curve is observed which levels off at a constant value at high q. This is the well-known Holtzer plateau πM_L which allows the determination of the length per monomer via the known mass per repeating unit M_o

$$l = M_o/M_L \tag{2}$$

From Figure 7 we derive $M_L = 33\,400$. The data of fractions 1−3 yield similar results with values of $M_L = 34\,000 \pm 5\%$ corresponding to $l = 0.071$ nm. This value agrees well with l_δ and l_{SFM} determined in the dry state (see Table 1). So far the length per monomer could be derived without the detailed model calculation of the particle scattering factor. We merely had to confine ourselves to the analysis of those data that belong to the normally eluting part of the chromatogram. "Normally eluting" means that the chain length distribution within a single elution slice of 0.06 mL is monomodal with a polydispersity $M_w/M_n < 2$. It will be shown in the Appendix that for bimodal chain length distributions of extremely large polydispersity too small values of the Holtzer plateau may be experimentally observed. For the data in the anomalous elution regime this is experimentally confirmed as shown by the solid circles in Figure 7.

At present the origin of the observed small length per monomer is difficult to discuss. Certainly a helix formation would lead to a smaller contour length. This would require the main chain to exhibit a pronounced tacticity which could not be detected by high-resolution NMR.[16] Alternatively, the steric overcrowding of the side chains could force the main chain into well-defined gauche/trans sequences, which, however, are not likely to lead to a perfect helix. For monodendron jacketed polymers the solid-state structure was proven by elaborate X-ray diffraction experiments to consist of helical arrangements of the side chains, however, with no detectable order of the main chain.[19−21] Therefore, the reduced contour length for the monodendron jacketed polymers was explained by a "random helix formation".[7] In view of simulations[22] and scaling arguments[23] on flexible polyelectrolytes claiming a persistent arrangement of locally coiled segments ("Gaussian blobs"), a similar scenario could be constructed for the cylindrical brushes as well. In fact, recent Monte Carlo simulations[24,25] of cylindrical brush molecules demonstrate the bond angle correlation function to exhibit two decay constants which, however, were not evaluated in a systematic manner. In the present state of investigation a quantitative comparison with the experiments is not meaningful, because the intrinsic stiffness, i.e., unperturbed Kuhn length, is not accounted for in the Monte Carlo simulations. As a consequence, the MC simulations observe a much smaller increase of the persistence length of the main chain, if the size of main and side chain monomers are identical, in clear disagreement with the experimental results. The problem of the reduced contour length for polymacromonomers has not yet been addressed directly by theory or simulations but becomes qualitatively evident from pictures of simulated structures.[26−28] We currently believe that no regular, i.e., helical, structure of the main chain is required in order to induce the cylindrical structure of the brush molecules. Rather, the steric interaction of the side chain may straighten out locally coiled segments which might not at all exhibit a significant helicity.

Determination of the Chain Stiffness. A precise analysis of the shape of the scattering curves principally allows the determination of the "true" radius of gyration, the Kuhn statistical segment length, and the polydispersity within a single elution slice. However, there are three major obstacles to overcome: (i) Due to the scatter of the experimental data, a fit with model calculations for the particle scattering factor might not be unique. In the present problem this ambiguity is significantly reduced because one set of parameters should fit several scattering curves. (ii) Since the molar mass distribution within a single elution slice is unknown, we have to assume a chain length distribution function in the model calculation. Here we have utilized a Schulz−Zimm distribution with variable convolution parameter m. (iii) The particle scattering factor for semiflexible polymers

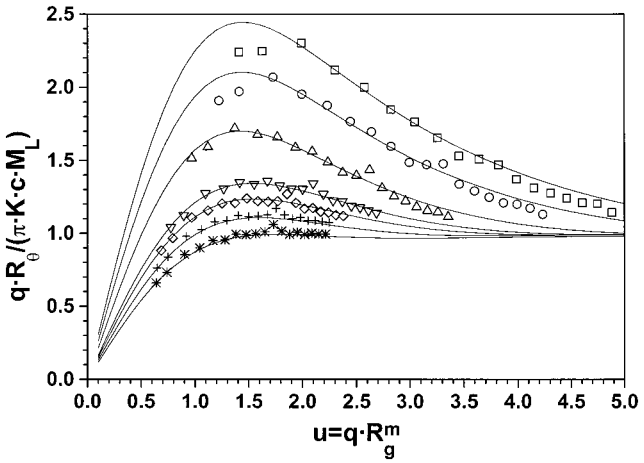

Figure 8. Normalized Holtzer plots $qR_\Theta/(KcM_L\pi)$ versus $u = qR_g^m$ as described in the text. Symbols are like in Figure 7; the solid lines represent the theoretical curves with L_w/l_k and m values as listed in Table 2.

of finite length is not yet precisely known. We adopt the approximate model introduced by Koyama[29] which was successfully employed in earlier investigations.[30,31]

To practically start with the theoretical modeling of the scattering curve, we have to introduce a better estimate for the quantity u instead of u_{app}. This is crudely achieved (±10%) by rescaling u_{app} in Figure 8 such that the maximum of the curves is located at $u = 1.55$, because model calculations have shown the maximum to shift from $u = 1.4$ for monodisperse ($m = \infty$) to $u = 1.7$ for Schulz−Flory distributed samples ($m = 1$).[31]

The next step involves a direct comparison of the theoretical to the experimental curves. The height of the maximum is proportional to the number of Kuhn statistical segments per chain, and the maximum becomes broader with increasing polydispersity. Since the convolution parameter m also determines the precise position of the maximum, the true radius of gyration is easily evaluated once m is known. The result is shown in Figure 8, where the normalized curves $qP(q)\cdot L_w/\pi = q(R_\Theta/Kc)/(M_L\pi)$ are plotted vs $u = qR_g^m$ with R_g^m the radius of gyration derived from the position of the maximum at fixed (and at least approximately known) convolution parameter m. The coincidence of experimental data and theoretical curves is almost perfect in view of the fact that deviations are magnified in the Holtzer plot. In practice, it was sufficient to create three sets of theoretical curves with $m = \infty$, $m = 8$, and $m = 4$ corresponding to $M_w/M_n = 1.0$, 1.125, and 1.25, respectively, each consisting of 20 L_w/l_k values between 0.1 and 15.

The resulting values for L_w/l_k and R_g^m obtained by comparison of the experimental to the theoretical curves are listed in Table 2 for selected elution slices of the unfractioned sample and of fractions 1−3.

The next step involves the determination of L_w and l_k at given L_w/l_k, R_g^m, and m. Utilizing the expression for R_g of a polydisperse wormlike chain[30,32]

$$R_g^2 = \frac{m+2}{6y}l_k - \frac{l_k^2}{4} + \frac{y l_k^3}{4(m+1)} - \frac{l_k^4}{8m(m+1)}\left(y^2 - \frac{y^{m+2}}{(y+2/l_k)^m}\right) \quad (4)$$

with $y = (m+1)/L_w$. Then L_w and l_k were varied at fixed L_w/l_k and m until the calculated radius of gyration, R_g^c, is equal to R_g^m. This procedure consistently yields $l_k = 120$ nm. Only for the smallest molar masses in each of the samples which are close to the anomalous elution regime are large deviations of R_g^m and R_g^c observed which are marked by stars in the first column of Table 2.

As shown in the Appendix, these deviations are most probably caused by the onset of anomalous elution, i.e., the occurrence of a bimodal chain length distribution within a single elution slice. We now utilize the values of the contour length and the mass per unit length M_L in order to calculate the true molar mass of the eluting molecules, which is also included in Table 2. Comparison of the true with the apparent quantities reveal huge differences of up to 30% and 40% for M_w and R_g, respectively, despite the apparent linearity of the experimental Zimm plots. To elucidate these subtle effects, three of the data sets shown in Figure 8 were replotted as $P(q)^{-1}$ vs u^2. In Figure 9 the solid line represents the wormlike chain fit whereas the broken line shows the linear regression. In fact, the linear regression is seen to be hardly worse than the wormlike chain fit but yields extremely wrong M_w and R_g values for the high molar mass samples. In the anomalous elution regime the calculated M_w^c becomes wrong because L_w/l_k is too small as outlined in the Appendix. For this reason M_w^{app} and M_w^c almost never agree.

The quantitative value for the chain stiffness $l_k = 120$ nm is significantly larger than determined for polymacromonomers with polystyrene side chains of similar length, which is counterintuitive because the styrene is more voluminous than the methacrylate monomer. This is simply explained by the fact that in the earlier investigation[2] the contour length was derived utilizing a length per monomer of $l = 0.25$ nm. Accordingly, the values reported earlier represent the lower limit of the chain stiffness.

Conclusion

Polymacromonomers consisting of methacryloyl end-functionalized oligomethacrylates exhibit a cylindrical structure that is characterized by an enormously high chain stiffness, i.e., $l_k = 120$ nm. This stiffening is caused solely by steric overcrowding of the densely packed side chains. The incompatibility of main and side chains in earlier investigated polymacromonomers with a polymethacrylate main chain and polystyrene side chains[1,2] does not have a significant influence on the chain stiffness.

For the first time the length per monomer of the cylindrical brush molecules has been determined in solution to $l = 0.071$ nm, which is much smaller than the maximum value of $l = 0.25$ nm for vinylic main chains. The contour length of the molecules in the dry state observed by AFM yields similarly small values for l, thus confirming earlier observations on poly(vinylpyridine) brushes[3] and on monodendron jacketed linear chains.[7] This allows the important conclusion that the reduction of the contour length as compared to its maximum value does not occur during the drying process in the first place but exists in solution as well. The limitations of SFM to monitor ensemble properties for samples exhibiting a very broad chain length distribution and the inaccuracy of the light scattering results, if only sub-milligram amounts of sample are

Table 2. Summary of the GPC/MALLS Results As Described in the Text[e]

sample	V_e/mL	$M_w^{app} \times 10^6$/ g mol^{-1} [a]	R_g^{app}/nm[a]	R_g^m/nm[b]	L_w/l_k[b]	m[b]	$M_w^c \times 10^6$/ g mol^{-1} [c]	R_g^c/nm[d]
unfractionated	16.8	72.6	230	150	14.0	0	57.0	174
	17.0	50.5	190	130	10.0	0	40.6	144
	17.3	30.2	144	103	6.0	0	24.5	106
	18.0	15.1	94	82.5	3.5	8	14.2	81
	18.3	12.0	81	73	2.7	8	11.0	68
	18.7	*10.0*	*73*	*69*	*2.0*	*8*	*8.1*	*55*
	19.0	*8.4*	*68*	*68*	*1.0*	*8*	*4.1*	*33*
fraction 1	16.8	32	142	115	7.5	8	30.5	129
	17.0	27	130	102	5.8	0	23.5	104
	17.3	21.4	113	100	4.75	8	16.1	98
	17.7	18.3	101	92	4.2	8	17.1	91
fraction 2	17.2	20.3	104	98	4.75	4	19.4	103
	17.4	17.0	95	90	3.75	4	15.3	89
	17.8	*12.7*	*80*	*73*	*2.3*	*8*	*9.4*	*61*
	18.2	*9.8*	*67*	*63*	*1.6*	*8*	*6.5*	*47*
fraction 3	17.3	29.0	126	110	8.0	4	32.5	141
	17.5	21.3	109	95	5.0	8	20.4	101
	17.8	16.0	93	82	3.5	8	14.2	81
	18.0	13.2	84	77.5	3.0	4	12.2	77.5
	18.3	*9.6*	*70*	*67*	*1.6*	*8*	*6.5*	*47*

[a] Determined by Zimm plots. [b] Determined by Holtzer analysis. [c] Calculated from L_w/l_k with $l_k = 120$ nm, $M_0 = 2410$ g mol^{-1}, and $l = 0.071$ nm. [d] Calculated according to eq 4. [e] The italic data could not be reliably fitted because of the onset of anomalous elution (see Appendix).

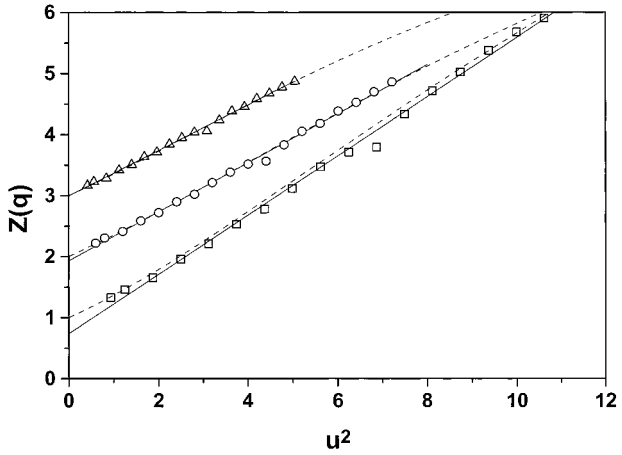

Figure 9. Zimm plots $Z(q) = 1/P(q) + a$ of some selected scattering data showing the linear regression errors. For clarity the curves are shifted by a constant a: $V_e = 16.8$ mL (□, $a = 0$); $V_e = 17.0$ mL (○, $a = 1$); and $V_e = 17.3$ mL (△, $a = 2$).

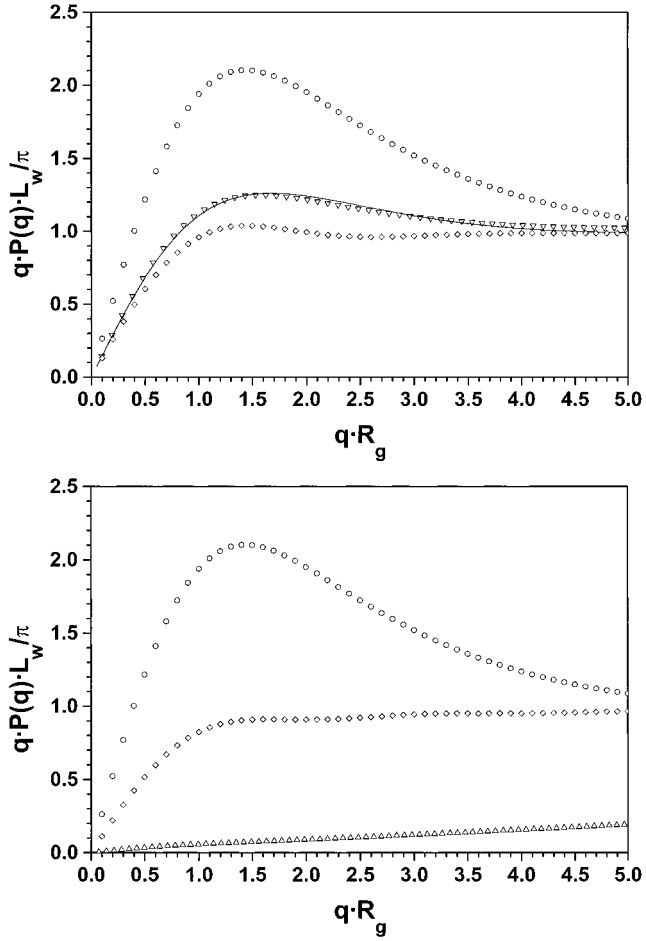

Figure 10. Theoretical Holtzer plots for semiflexible chains exhibiting a bimodal chain length distribution: (a) $L_1/l_k = 10$ (○), $L_2/l_k = 1$ (◇), $m_1 = m_2 = 0.5$ (▽); (b) $L_1/l_k = 10$ (○), $L_2/l_k = 0{,}1$ (◇), $m_1 = 0.01$ (△).

available, prohibit a more quantitative comparison of the contour length of the cylindrical brushes in the dry and dissolved state. Accordingly, future investigations will focus on more perfect fractionations, i.e., obtain a larger amount of sample with a significantly reduced polydispersity of the chain length.

The anomalous elution of high molar mass polymacromonomers has been detected by GPC/MALLS and could be reduced to a delayed elution of an extremely high molar mass fraction of the sample. The origin of the retardation, however, remains unclear.

Acknowledgment. The financial support from Deutsche Forschungsgemeinschaft, Fonds der Chemischen Indusrie, and the Materials Science Center of the University of Mainz is gratefully acknowledged.

Appendix

To investigate the effect of a bimodal chain length distribution in the Holtzer plot, two model calculations are performed. In Figure 10a the Holtzer plots for two monodisperse wormlike chains of $L_1/l_k = 10$ and $L_2/l_k = 1$ are shown together with the curve for the mixture of both with identical mass fractions $m_1 = m_2 = 0.5$. The solid line represents the best fit to the mixture utilizing the theoretical calculation of the form factor

with a monomodal Schulz−Zimm chain length distribution. The fit parameters are $L_w/l_k = 3.3$ and $m = 3$ (yielding $L_w/L_n = 1.33$) which ought to be compared to the true values $L_w/l_k = 5.5$ and $L_w/L_n = 3$. The fitted contour length L_w is clearly too small, which perfectly explains the discrepancy between the R_g^c and R_g^m values observed at higher elution volumes listed in Table 2 in the text.

The second calculation addresses the experimental results obtained in the regime of anomalous elution, one example of which is included in Figure 7. Here, the chain length distribution is expected to be bimodal with extremely large polydispersities. Therefore, in Figure 10b the Holtzer plot of two monodisperse samples with $L_1/l_k = 10$ and $L_2/l_k = 0.1$ are shown together with the scattering curve for the mixture with mass fraction $m_1 = 0.01$. Within the experimentally accessible regime the Holtzer plateau is never reached. Both examples clearly impose strong limitations to the applicability of the data analysis proposed above. It should be noted, however, that the apparent Holtzer plateau obtained for extremely bimodal distributions would lead to unphysically small M_L values, i.e., too large l values.

References and Notes

(1) Wintermantel, M.; Schmidt, M.; Tsukahara, Y.; Kajiwara, K.; Kohjiya, S. *Macromol. Rapid Commun.* **1994**, *15*, 279.
(2) Wintermantel, M.; Gerle, M.; Fischer, K.; Schmidt, M.; Wataoka, I.; Urakawa H.; Kajiwara, K.; Tsukahara, Y. *Macromolecules* **1996**, *29*, 978.
(3) Dziezok, P.; Sheiko, S. S.; Fischer, K.; Schmidt, M.; Möller, M. *Angew. Chem.* **1997**, *109*, 2894.
(4) Sheiko, S. S.; Gerle, M.; Fischer, K.; Schmidt, M.; Möller, M. *Langmuir* **1997**, *13*, 5368.
(5) Percec, V.; Ahn, C.-H.; Ungar, G.; Yeardley, D. S. P.; Möller, M.; Sheiko, S. S. *Nature (London)* **1998**, *391*, 161.
(6) Karakaya, B.; Claussen, W.; Gessier, K.; Sänger, W.; Schlüter, A.-D. *J. Am. Chem. Soc.* **1997**, *119*, 3296.
(7) Prokhorova, S. A.; Sheiko, S. S.; Möller, M.; Ahn, C.-H.; Percec, V. *Macromol. Rapid Commun.* **1998**, *19*, 359−366.
(8) Radke, W.; Müller, A. H. E. *Makromol. Chem., Macromol. Symp.* **1992**, *54/55*, 583.
(9) Tsukahara, Y.; Kohjiya, S.; Tsutsumi, K.; Okamoto, Y. *Macromolecules* **1989**, *22*, 1546.
(10) Tsukahara, Y.; Tsutsumi, K.; Yamashita, Y.; Shimada, S. *Macromolecules* **1990**, *23*, 5201.
(11) Wintermantel, M.; Antonietti, A.; Schmidt, M. *J. Appl. Polym. Sci., Polym. Symp.* **1993**, *52*, 91.
(12) Zhong, Q.; Inniss, D.; Ellings, V. B. *Surf. Sci.* **1993,** *290*, L688.
(13) Radmacher, M.; Fritz, M.; Kacher, C. M.; Cleveland, J. P.; Hansma, P. K. *Biophys. J.* **1996,** *70*, 556.
(14) Winkler, R. G.; Spatz, L. P.; Sheiko, S. S.; Möller, M.; Reineker, P.; Marti, O. *Phys. Rev. B* **1996**, *54*, 8908.
(15) Burnham, N. A.; Behrend, O. P.; Oulevey, F.; Gremaud, G.; Gallo, P.-J.; Gourdon, D.; Dupas, E.; Kulik, A. J.; Pollock, H. M.; Briggs, G. A. D. *Nanotechnology* **1997**, *8*, 2.
(16) Gerle, M. Ph.D. Thesis, Mainz, 1998.
(17) Percec, V.; Ahn, C.-H.; Cho, W.-D.; Jamieson, A. M.; Kim, J.; Leman, T.; Schmidt, M.; Gerle, M.; Möller, M.; Prokhorova, S. A.; Sheiko, S. S.; Cheng, S. Z. D.; Zhang, A.; Ungar, G.; Yeardley, D. J. P. *J. Am. Chem. Soc.* **1998**, *120*, 8619.
(18) Hofe, T. Ph.D. Thesis, Mainz, 1997.
(19) Kwon, Y. K.; Chvalun, S.; Schneider, A.-I.; Blackwell, J.; Percec, V.; Heck, J. A. *Macromolecules* **1994,** *27*, 6129.
(20) Kwon, Y. K.; Chvalun, S. N.; Blackwell, J.; Percec, V.; Heck, J. A. *Macromolecules* **1995,** *28*, 1552.
(21) Kwon, Y. K.; Danko, C.; Chvalun, S.; Blackwell, J.; Heck, J. A.; Percec, V. *Macromol. Symp.* **1994**, *87*, 103.
(22) Stevens, M. J.; Kremer, K. *Macromolecules* **1993**, *26*, 4717.
(23) Dobrynin, A. V.; Colby, R. H.; Rubinstein, M. *Macromolecules* **1995**, *28*, 1859.
(24) Rousault, Y.; Borisov, O. V. *Macromolecules* **1996**, *29*, 2605.
(25) Saariaho, M.; Szleifer, I.; Ikkala, O.; ten Brinke, G. *Macromol.-Theory Simul.* **1998**, *7*, 211.
(26) Saariaho, M.; Ikkala, O.; Szleifer, I.; Erukhimovich, I.; ten Brinke, G. *J. Chem. Phys.* **1997,** *107*, 3267.
(27) Schlüter, A. D. *Top. Curr. Chem.* **1998**, *197*, 165.
(28) Stocker, W.; Schürmann, B. L.; Rabe, J. P.; Förster, S.; Lindner, P.; Neubert, I.; Schlüter, A. D. *Adv. Mater.* **1998**, *10*, 793.
(29) Koyama, R. *J. Phys. Soc. Jpn.* **1973**, *34*, 1029.
(30) Schmidt, M. *Macromolecules* **1984**, *17*, 553.
(31) Schmidt, M.; Paradossi, G.; Burchard, W. *Makromol. Chem., Rapid Commun.* **1985**, *6*, 767.
(32) Oberthür, R. C. *Makromol. Chem.* **1978**, *179*, 2693.

MA9816463